the plant journal

SEB Society for Experimental Biology

The Plant Journal (2017) **92,** 939–950 doi: 10.1111/tpj.13730

Multifaceted plant responses to circumvent Phe hyperaccumulation by downregulation of flux through the shikimate pathway and by vacuolar Phe sequestration

Joseph H. Lynch[1], Irina Orlova[2,†], Chengsong Zhao[3], Longyun Guo[1], Rohit Jaini[4], Hiroshi Maeda[2,‡], Tariq Akhtar[5,§], Junellie Cruz-Lebron[1], David Rhodes[2], John Morgan[1,4], Guillaume Pilot[3], Eran Pichersky[5] and Natalia Dudareva[1,2,6,*]

[1]*Department of Biochemistry, Purdue University, West Lafayette, IN 47907, USA,*
[2]*Department of Horticulture and Landscape Architecture, Purdue University, West Lafayette, IN 47907, USA,*
[3]*Department of Plant Pathology, Physiology, and Weed Science, Virginia Tech, Blacksburg, VA 24061, USA,*
[4]*School of Chemical Engineering, Purdue University, West Lafayette, IN 47907, USA,*
[5]*Department of Molecular, Cellular and Developmental Biology, University of Michigan, Ann Arbor, MI 48109, USA, and*
[6]*Purdue Center for Plant Biology, Purdue University, West Lafayette, IN 47907, USA*

Received 9 December 2016; revised 10 July 2017; accepted 28 September 2017; published online 4 November 2017.
*For correspondence (e-mail dudareva@purdue.edu).
†Present address: The Scotts Miracle-Gro Company, Marysville, OH 43041, USA.
‡Present address: Department of Botany, University of Wisconsin – Madison, Madison, WI 53706-1313, USA.
§Present address: Department of Molecular and Cellular Biology, University of Guelph, Guelph, Ontario Canada N1G 2W1.

SUMMARY

Detrimental effects of hyperaccumulation of the aromatic amino acid phenylalanine (Phe) in animals, known as phenylketonuria, are mitigated by excretion of Phe derivatives; however, how plants endure Phe accumulating conditions in the absence of an excretion system is currently unknown. To achieve Phe hyperaccumulation in a plant system, we simultaneously decreased in petunia flowers expression of all three Phe ammonia lyase (PAL) isoforms that catalyze the non-oxidative deamination of Phe to *trans*-cinnamic acid, the committed step for the major pathway of Phe metabolism. A total decrease in PAL activity by 81–94% led to an 18-fold expansion of the internal Phe pool. Phe accumulation had multifaceted intercompartmental effects on aromatic amino acid metabolism. It resulted in a decrease in the overall flux through the shikimate pathway, and a redirection of carbon flux toward the shikimate-derived aromatic amino acids tyrosine and tryptophan. Accumulation of Phe did not lead to an increase in flux toward phenylacetaldehyde, for which Phe is a direct precursor. Metabolic flux analysis revealed this to be due to the presence of a distinct metabolically inactive pool of Phe, likely localized in the vacuole. We have identified a vacuolar cationic amino acid transporter (*PhCAT2*) that contributes to sequestering excess of Phe in the vacuole. *In vitro* assays confirmed PhCAT2 can transport Phe, and decreased *PhCAT2* expression in *PAL*-RNAi transgenic plants resulted in 1.6-fold increase in phenylacetaldehyde emission. These results demonstrate mechanisms by which plants maintain intercompartmental aromatic amino acid homeostasis, and provide critical insight for future phenylpropanoid metabolic engineering strategies.

Keywords: phenylalanine ammonia lyase, phenylalanine, phenylpropanoids, aromatic amino acids, shikimate pathway, *Petunia hybrida*, regulation.

INTRODUCTION

In mammals, hyperaccumulation of phenylalanine (Phe) leads to phenylketonuria (PKU), a degenerative neurological disorder that arises from a loss of Phe hydroxylase activity (Williams *et al.*, 2008). The buildup of Phe to toxic levels in PKU results in its conversion to phenylpyruvic acid and its derivatives, which are excreted with urine. Microbes prevent such accumulations through catabolism back to central carbon metabolism (Fuchs *et al.*, 2011). However, how plants tolerate high Phe levels in the absence of analogous excretion or catabolic systems remains unknown.

Under normal growth conditions, plants direct 20–30% of photosynthetically fixed carbon towards the shikimate pathway (Haslam, 1993) and subsequently to biosynthesis

of aromatic amino acids with the highest flux to Phe. In addition to being a building block for protein biosynthesis, Phe serves as a precursor for a multitude of phenolic compounds that have prominent, and often vital, roles in plant growth and development (e.g. lignin, suberin), reproduction (e.g. phenylpropanoids, benzenoids) and defense (e.g. salicylic acid, tannins, flavonoids). Constituting approximately 30–45% of plant organic matter (Razal *et al.*, 1996), Phe-derived products are primarily synthesized in the cytosol but rely predominantly on Phe biosynthesis in and its export out of plastids (Maeda and Dudareva, 2012; Widhalm *et al.*, 2015).

In plants, Phe hyperaccumulation could be achieved by mutations in L-Phe ammonia lyase (PAL, EC 4.3.1.5; Rohde *et al.*, 2004), which catalyzes the first committed step, the non-oxidative deamination of Phe to *trans*-cinnamic acid, in the general phenylpropanoid pathway. PAL controls the carbon flux toward phenylpropanoid compounds and is often encoded by a small multigene family with four members in *Arabidopsis thaliana* (Raes *et al.*, 2003) and *Nicotiana tabacum* (Reichert *et al.*, 2009), and three members in *Petunia hybrida* (Colón *et al.*, 2010). Expression of *PAL* genes is differentially and developmentally regulated, and is induced by biotic and abiotic stresses (Zhang and Liu, 2015). Over the last decade, it has been shown that disruption of PAL activity leads to a decrease in downstream phenylpropanoid metabolism (Rohde *et al.*, 2004; Huang *et al.*, 2010; Shi *et al.*, 2010; Song and Wang, 2011; Kim and Hwang, 2014; Cass *et al.*, 2015). However, the effect of accompanying Phe hyperaccumulation on Phe homeostasis is currently unknown.

Here we limited Phe utilization in *P. hybrida* cv. Mitchell flowers by decreasing PAL activity via RNAi technology, and investigated its effects on upstream and downstream Phe metabolism. To avoid possible detrimental effects on plant vitality, a problem previously encountered upon systemic PAL perturbations in Arabidopsis (Huang *et al.*, 2010), metabolic manipulations were achieved specifically in the flowers by using a petal-specific promoter. Petunia flowers have high carbon flux through the phenylpropanoid network and emit high levels of exclusively Phe-derived volatiles (Verdonk *et al.*, 2003; Boatright *et al.*, 2004). They also contain phenylacetaldehyde synthase (PAAS) that catalyzes phenylacetaldehyde formation directly from Phe and thus competes with PAL for Phe utilization (Kaminaga *et al.*, 2006). The current results show that Phe hyperaccumulation affects carbon flux through the shikimate pathway and towards aromatic amino acids to maintain cytosolic Phe homeostasis. Similar flux redistribution occurs in Arabidopsis quadruple *pal* mutants, suggesting that these metabolic changes are not unique to petunia flowers. Moreover, excess Phe is not redirected towards phenylacetaldehyde formation, but rendered metabolically inactive by sequestration in the vacuole. Decreasing the expression of a newly identified *P. hybrida* vacuolar cationic amino acid transporter (PhCAT2) counteracts Phe sequestration in the vacuole of *PAL*-RNAi plants and makes it available to cytosolic enzymes.

RESULTS

Phe hyperaccumulation perturbs not only phenylpropanoid metabolism but also aromatic amino acid biosynthesis

Previously we showed that petunia flowers, which produce high levels of phenylpropanoid/benzenoid volatiles, express three PAL isoforms (Colón *et al.*, 2010). While all three isoforms are highly similar in sequence (Figure S1), PAL1 displays the highest expression in petunia petals 2 days post-anthesis, the stage of development with the highest levels of volatile phenylpropanoids, and PAL3 exhibits the lowest transcript level (Colón *et al.*, 2010). To achieve Phe hyperaccumulation and to identify the role of PAL in the regulation of Phe metabolism, we simultaneously decreased the expression of all three PAL genes in petunia by using a single RNAi construct (Figure S2a) under control of a petal-specific promoter (Cseke *et al.*, 1998). Out of multiple independent lines, two lines (11 and 26) showing the greatest reduction in *PAL* expression were selected for further metabolic profiling. Based on quantitative reverse transcriptase-polymerase chain reaction (qRT-PCR) with gene-specific primers, in line 11 expressions of *PAL1*, *PAL2*, and *PAL3* were reduced by 98.5%, 92.0% and 93.5%, respectively, while their levels were decreased by 97.5%, 89.7% and 96.6%, respectively, in line 26 relative to control wild-type flowers (Figure S2b), which were metabolically indistinguishable from empty vector control (Figure S3). *RNAi-PAL* suppression reduced PAL activity by 94% and 81% for lines 11 and 26, respectively, relative to controls (Figure 1). Flowers of the transgenic lines had a slight but statistically significant decrease in fresh weight relative to wild-type (Figure 1), otherwise the plants appeared morphologically unchanged.

Transgenic petals of both lines had 18-fold higher levels of Phe than wild-type, and drastically diminished emission of volatiles derived from *trans*-cinnamic acid (Figure 1). Emission of all phenylpropanoids/benzenoids was reduced in both transgenic lines relative to control, including an 85–99.5% reduction in emission benzaldehyde, benzylalcohol, benzylbenzoate, phenylethylbenzoate, methylbenzoate, eugenol and isoeugenol (Figure 1). Methylsalicylate emission was reduced by 47–65% in transgenic lines (Figure 1).

Reduction in PAL activity in both *PAL*-RNAi lines led to accumulation of Tyr and Trp, with levels increasing on average by 6.3- and 5.5-fold, respectively (Figure 1). Unexpectedly, the level of shikimic acid was significantly reduced in both transgenic lines relative to controls

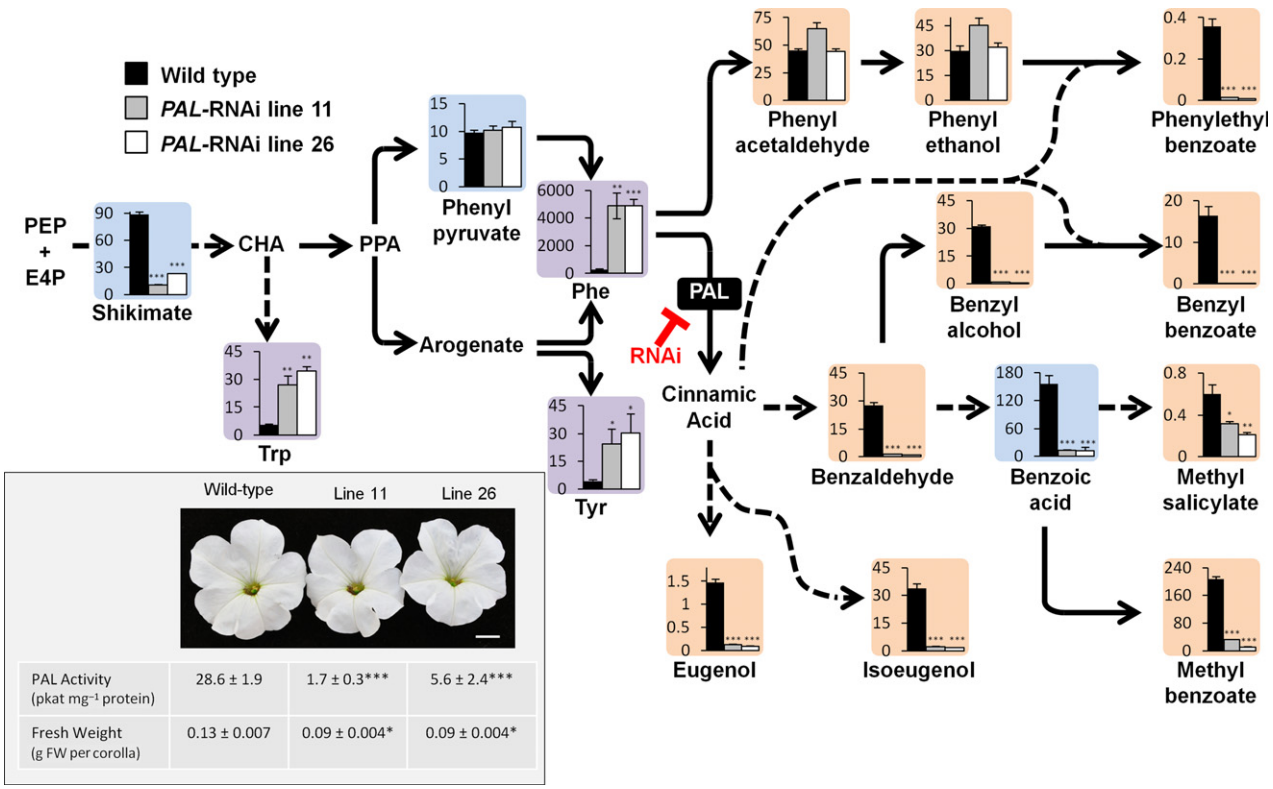

Figure 1. Effect of *PAL*-RNAi suppression on flower morphology and aromatic amino acid and phenylpropanoid/benzenoid metabolism.
Emitted volatiles (orange background) were collected from 20:00 to 08:00 h, and internal pools of organic (blue background) and aromatic amino acids (purple background) were extracted at 20:00 h from control (black bars) and transgenic petunia *PAL*-RNAi lines 11 (gray bars) and 26 (white bars) flowers 2 days post-anthesis. Results are presented as nmol gFW^{-1} h^{-1} for emitted volatiles and nmol gFW^{-1} for internal pools. Data are means ± SE of a minimum of three biological replicates. Inset: representative flowers of wild-type and *PAL*-RNAi lines 11 and 26 show a discernable decrease in flower size in RNAi lines relative to wild-type (scale bar: 1 cm). Phe ammonia lyase (PAL) activity and corolla fresh weights are given as the average ± SE. $*P < 0.05$, $**P < 0.01$, $***P < 0.001$.

(by 74–88%), while phenylpyruvate level remained unchanged (Figure 1).

Reduction in PAL activity decreases carbon flux through the shikimate pathway

To determine changes in flux through the shikimate pathway, wild-type and line 11 petunia flowers were fed with uniformly ^{13}C-labeled ([U-$^{13}C_6$]) glucose, and pool sizes and isotopic abundances of glucose, shikimate and aromatic amino acids were analyzed at different time points over a 4-h period. The glucose labeling pattern was nearly identical in both control and transgenic petals (Figure 2). In both genotypes, glucose labeling always exceeded labeling of shikimate, consistent with a simple precursor–product relationship between sucrose and shikimate (Figure S4). Over this time course, the shikimate pool was significantly reduced in transgenic petals relative to the control, while there was little difference in its isotopic labeling (Figure S4). We have constructed a dynamic model of the aromatic amino acid biosynthetic network to reproduce the observations from ^{13}C-labeled glucose feeding for both wild-type and *PAL*-RNAi flowers. Shikimate pathway flux estimated by the model was found to be 50.9% less in *PAL*-RNAi than wild-type (Table 1). There is a corresponding decrease of 50.9% in flux towards Phe, while the fluxes toward Tyr and Trp are increased by 78.6% and 75.0%, respectively.

To assess whether the observed changes in flux through the shikimate pathway are the result of decreased expression of 3-deoxy-D-*arabino*-heptulosonate 7-phosphate synthase (DAHPS), which catalyzes the first committed step in the shikimate pathway (Bentley, 1990; Herrmann and Weaver, 1999), *DAHPS* transcript levels were analyzed in petals of two transgenic petunia lines and control plants. In addition, we examined the expression of genes downstream of shikimate (e.g. 5-enolpyruvylshikimate 3-phosphate synthase, EPSPS) and those involved in Phe and Tyr biosynthesis (chorismate mutase, CM1, and arogenate dehydratases, ADT1, ADT2 and ADT3), as well as the expression of the shikimate pathway transcriptional regulator, ODORANT1 (ODO1; Verdonk *et al.*, 2005). No statistically significant changes in *DAHPS*, *EPSPS*, *CM1* and *ODO1* transcript levels were observed in transgenic flowers relative to controls, although *ODO1* expression exhibited an apparent decreasing trend (Figure S5a). Transcript

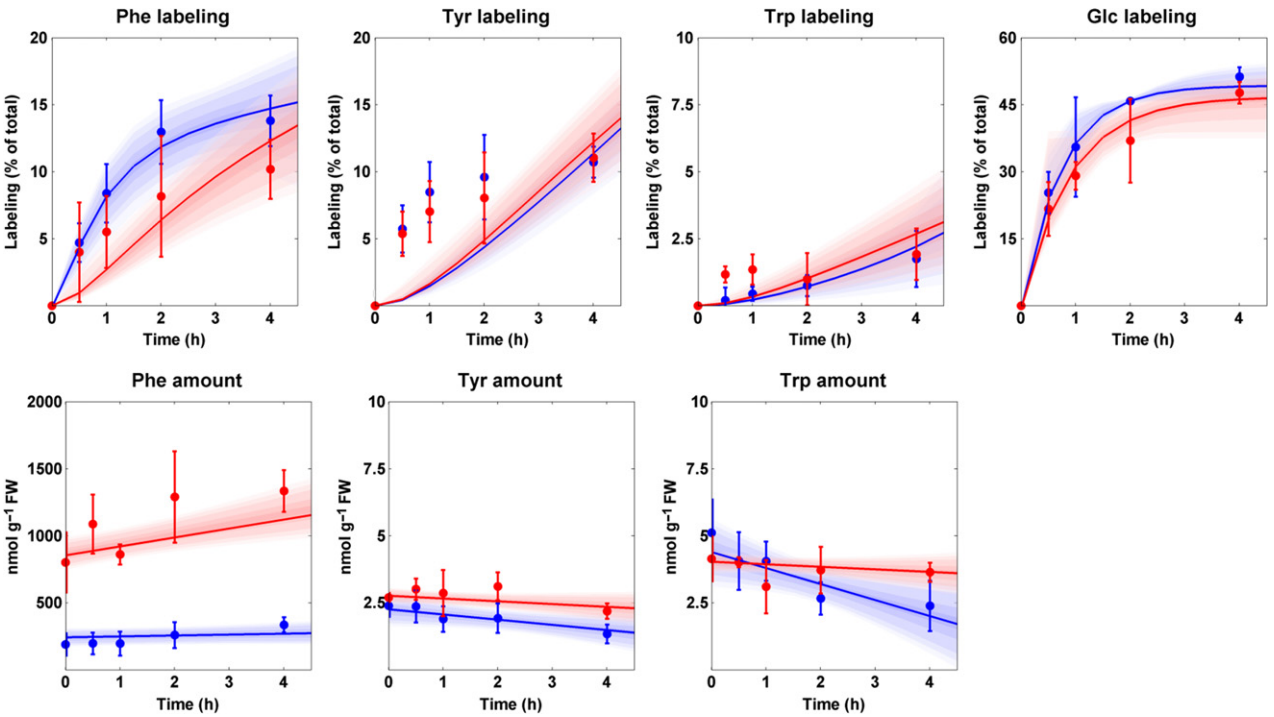

Figure 2. Dynamic model simulation and experimentally obtained pool sizes and labeling patterns for aromatic amino acids and glucose in wild-type and *PAL*-RNAi petunia flowers.
Isotopic abundances and pool sizes were analyzed over a 4-h time period (starting at 18:00 h) of [U-$^{13}C_6$]-glucose feeding to flowers of control (blue lines and symbols) and transgenic *PAL*-RNAi line 11 (red lines and symbols) plants. Lines represent simulation results, with the shaded area reflecting 95% confidence area for model's outputs. Data points are the average of three biological replicates, error bars represent standard deviation.

Table 1 Model-predicted metabolic fluxes within the aromatic amino acid biosynthetic network

	Biosynthetic fluxes (nmol gFW^{-1} h^{-1})				
	Phe	Tyr	Trp	Shik	Inactive Phe (nmol gFW^{-1})
Wild-type	456.6 ± 91.4	0.14 ± 0.02	0.04 ± 0.01	456.8 ± 91.4	188.5 ± 26.8
PAL-RNAi	224.2 ± 37.2	0.25 ± 0.05	0.07 ± 0.03	224.5 ± 37.2	830.9 ± 71.7
Relative change	−50.9%	+78.6%	+75.0%	−50.9%	+340.8%

All parameter means and variances were obtained based on the values estimated from 5000 synthetic datasets fit to experimentally determined label incorporation from exogenously supplied [U-$^{13}C_6$]-glucose over 4 h, as described in Supporting Methods.

levels of the most highly expressed petunia ADT gene, *ADT1*, remained unaffected in flowers of transgenic lines, while *ADT2* and *ADT3* expression was increased only in line 11 (Figure S5b). However, total ADT activity was unaltered in either transgenic line (Figure S5b).

Perturbations in aromatic amino acid biosynthesis following Phe hyperaccumulation in Arabidopsis stems mirror those of petunia petals

To determine whether the observed changes in the shikimate pathway flux and Phe biosynthesis as a result of Phe hyperaccumulation are unique to petunia petals, or if this might be a more general property of plants, we performed metabolic profiling of Arabidopsis stem from previously generated double *pal1pal2* and quadruple *pal1pal2pal3pal4* knockout mutants (Huang *et al.*, 2010). Similar to petunia petals, there is a high carbon flux toward phenylpropanoids in the Arabidopsis inflorescence stem, as it represents a major site of lignin biosynthesis. All four *PAL* genes are expressed in Arabidopsis stem, with *AtPAL-3* displaying the lowest expression (Raes *et al.*, 2003; Rohde *et al.*, 2004). Metabolic profiling revealed that similar to *PAL*-RNAi petunia petals, in Arabidopsis quadruple *pal1pal2pal3pal4* knockout mutants, the internal pools of three aromatic amino acids were drastically increased while shikimate level was decreased (Figure 3). The same trend was observed in double *pal1pal2* mutants, and the degrees of changes

were intermediate of wild-type and the quadruple mutants (Figure 3).

Decreased *PAL* expression leads to the accumulation of Phe that is metabolically inactive

Previously we have shown that petunia flowers produce phenylacetaldehyde by the action of a single cytosolic enzyme, PAAS, which catalyzes Phe decarboxylation-amine oxidation and competes with PAL for Phe utilization (Kaminaga *et al.*, 2006). We also showed that feeding of petunia flowers with a range of concentrations of $^{2}H_5$-Phe led to a proportional increase in the internal pools of phenylacetaldehyde and its derivative 2-phenylethanol (Colón *et al.*, 2010). Subsequently, a kinetic model of the petunia phenylpropanoid/benzenoid network was developed to simulate the network responses to different concentrations of supplied Phe (Colón *et al.*, 2010). Using this model, we predicted that although kinetic constraints do not enable PAAS activity to prevent Phe accumulation, the observed increase in Phe levels in the *PAL*-RNAi lines should result in up to a fourfold increase in phenylacetaldehyde emission (Figure S6a). However, no statistically significant changes were observed in phenylacetaldehyde and phenylethanol emission rates in transgenic lines relative to controls (Figure 1). This result was not due to a decrease in PAAS activity as it remained unchanged in transgenic plants (Figure S6b), suggesting that accumulated Phe is not accessible by PAAS in cytosol.

Moreover, feeding of petunia flowers from *PAL*-RNAi line 11 with uniformly labeled ^{13}C-glucose resulted in more rapid incorporation of label into the product, phenylacetaldehyde, than in its substrate, Phe (20.2% and 11.7% in 2 h, respectively; Figure 4a). The observed labeling patterns further suggested that within the cell there is an inaccessible largely unlabeled Phe pool, which based on constructed dynamic flux model of the aromatic amino acid biosynthetic network was increased by 341% in the *PAL*-RNAi line 11 relative to wild-type (Table 1). To determine the turnover of the metabolically inactive Phe pool, petunia petals were preloaded with ring-labeled $^{13}C_6$-Phe for 2 h (point 0 in Figure 4b) followed by a 6 h chase with unlabeled Phe, and intracellular Phe was analyzed for retention of the label. The $^{13}C_6$-Phe pool was depleted by 61% after 4 h of chase and remained unchanged thereafter. This lack of turnover further demonstrates that Phe is sequestered to a metabolically inactive pool.

Previous studies showed that Phe is present in vacuoles in Arabidopsis and barley plants (Krueger *et al.*, 2011; Tohge *et al.*, 2011). Thus, we hypothesized that the metabolically inactive Phe is located in the vacuole. To test this hypothesis, we analyzed Phe levels in vacuoles isolated from 1-day-old control and transgenic petunia flowers. Vacuole purity was verified by Western blot analysis with antibodies recognizing proteins specific to different subcellular compartments (Figure S7). Indeed, *PAL*-RNAi line 11 vacuoles exhibited a nearly twofold expansion in Phe content relative to wild-type vacuoles (Figure 5a). In addition, we looked for petunia vacuolar transporters that might be involved in amino acid homeostasis. During our recent study to identify and characterize a plastidial Phe exporter (Widhalm *et al.*, 2015), we also identified a contig, *Ph18042*, whose expression exhibited a twofold increase in petunia petals on day 2 post-anthesis relative to buds, the tissues with highest and lowest Phe levels, respectively. *Ph18042* was predicted to be localized to the vacuole and displays 71%/81% identity/similarity to Arabidopsis vacuolar cationic amino acid transporter, AtCAT2 (Su *et al.*, 2004; Yang *et al.*, 2014). In the current investigation, the full-length sequence of *Ph18042* was fused to the N-terminus of the green fluorescent protein (GFP) reporter protein and transformed in *A. thaliana* expressing the tonoplast marker *VAMP711*-mCHERRY (Geldner *et al.*, 2009) in order to experimentally determine its subcellular localization. Green fluorescence of the *Ph18042*-GFP in Arabidopsis leaf epidermis was co-localized with the red fluorescence of the tonoplast mCherry marker (Figure S8), suggesting that similar to Arabidopsis AtCAT2, Ph18042 (designated as PhCAT2) is localized in the tonoplast.

Neither PhCAT2 nor its more-studied homolog AtCAT2 have previously been directly tested for the ability to transport Phe. To test for the ability of PhCAT2 to transport Phe, it was overexpressed in *Saccharomyces cerevisiae* mutants with gene deletions for the endogenous vacuolar amino acid transporters AVT1, AVT3 and AVT4. Vacuolar

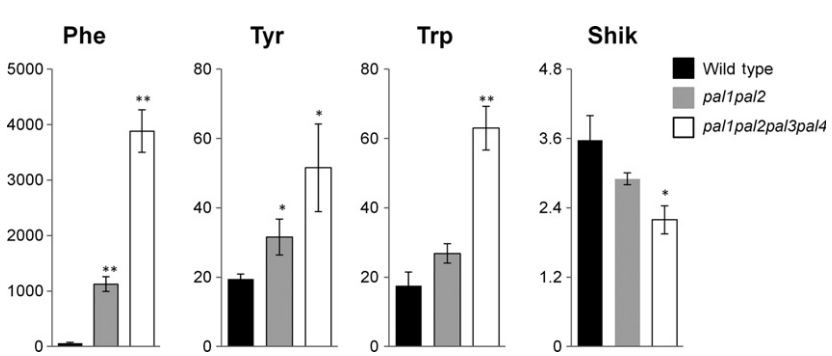

Figure 3. Levels of aromatic amino acids and shikimate in *pal1pal2* double and *pal1pal2pal3pal4* quadruple Arabidopsis mutants.
Black bar, wild-type control; gray bar, *pal1pal2* double mutants; white bar, *pal1pal2pal3pal4* quadruple mutants. Data are means ± SE ($n \geq 4$ biological replicates). *$P < 0.05$, **$P < 0.01$; Shik, shikimate.

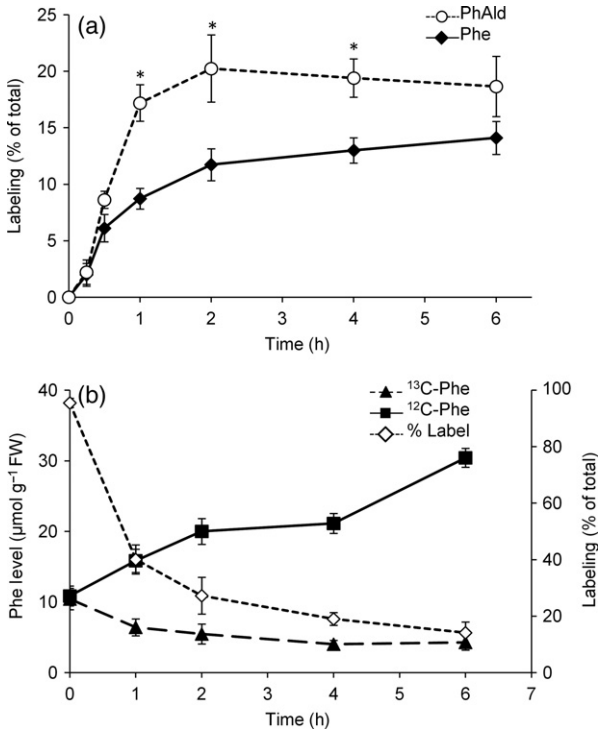

Figure 4. Isotopic labeling of Phe and phenylacetaldehyde from [^{13}C]-glucose and pulse/chase feeding of [^{13}C]-Phe/[^{12}C]-Phe to *PAL*-RNAi petunia flowers.

(a) Labeling kinetics of Phe and phenylacetaldehyde over a 6-h time period, beginning at 18:00 h, in *PAL*-RNAi line 11 flowers fed with [U-$^{13}C_6$]-glucose. Label incorportation into Phe is shown with black diamonds and into phenylacetaldehyde with white circles.

(b) Results of pulse-chase experiments. Flowers of *PAL*-RNAi line 11 were pre-fed for 2 h with 75 mM [$^{13}C_6$]-Phe before being transferred to 75 mM unlabeled Phe at time = 0 (18:00 h). Internal pools of labeled (black triangles) and unlabeled (black squares) Phe, as well as its isotopic abundance (white diamonds) were analyzed over a 6-h period. All data are means ± SE (n = 3 biological replicates). *$P < 0.05$ as determined by unpaired two-tailed Student's t-tests between phenylacetaldehyde and Phe labeling.

microsomes prepared from uncomplemented mutants were dramatically impaired in their ability to import Phe. However, PhCAT2 expression largely alleviated this impairment (Figure 5b). Omitting ATP in the assay abolished the transport (Figure S9), similar to the situation previously shown for yeast transporters (Russnak *et al.*, 2001), and for Phe uptake by isolated plant vacuoles (Homeyer and Schultz, 1988). Together, these results confirm that PhCAT2 is a bonafide vacuolar Phe transporter.

To examine whether PhCAT2 contributes to sequestering excess Phe in the vacuole and thereby precluding its availability in the cytosol for phenylacetaldehyde production, *PhCAT2* expression was transiently decreased in wild-type and *PAL*-RNAi line 11 petunia flowers using *PhCAT2*-RNAi construct. A 70% reduction in *PhCAT2* expression in wild-type flowers (Figure 5c) resulted in no increase in phenylacetaldehyde emission, indicating little, if any, change in cytosolic Phe availability under normal conditions (Figure 5d). In contrast, a similar reduction in *PhCAT2* expression in a *PAL*-RNAi line 11 resulted in a 1.6-fold increase in phenylacetaldehyde emission, providing *in vivo* evidence that PhCAT2 transports the excess Phe from the cytosol into the vacuole.

Phe hyperaccumulation leads to accumulation of new Phe-derived compounds

GC-MS metabolic profiling of trimethylsilyl-derived extracts revealed three peaks for which levels were increased 12–14-fold in the *PAL*-RNAi flowers relative to controls (Figure S10). ESI fragmentation patterns were nearly identical for two of the three unknown peaks, and all three contain fragments consistent with the presence of the benzyl moiety (m/z 179 and 193). Furthermore, feeding with ring-labeled $^2H_5$-Phe resulted in a +5 mass shift in the m/z 179 and 193 ions, indicating that these compounds contain an unsubstituted aromatic ring derived from Phe. However, neither fragmentation patterns nor total masses matched with known compounds cataloged in the NIST databases (Figure S10). Additional attempts to identify these compounds by MALDI-TOF and LC-TOF were unsuccessful. The levels of each of these three compounds were estimated based on total ion current relative to internal standard assuming a similar response factor for Phe-derived compounds. Their levels ranged from 3% to 5% of the elevated Phe content in *PAL*-RNAi flowers.

DISCUSSION

In petunia flowers, as in lignifying plant tissues, a substantial portion of total carbon metabolic flux is directed through PAL, which catalyzes the entry step into the phenylpropanoid pathway. While in lignifying tissues PAL activity sustains lignin formation and production of other phenylpropanoids, in petunia flowers it enables the extensive production of phenylpropanoid/benzenoid volatiles, and in some cultivars anthocyanins, for pollinator attraction. Previously, it has been shown in Arabidopsis that decreased PAL activity results in a buildup of Phe (Rohde *et al.*, 2004; Huang *et al.*, 2010) that is analogous to natural conditions in which aromatic amino acids accumulate in response to stress (Brouquisse *et al.*, 1992; Kim *et al.*, 2007; Saeedipour, 2012). We show here that plants could activate mitigating mechanisms to prevent potential detrimental effects of such buildup. Our results indicate that decreased Phe utilization in the cytosol has multifaceted intercompartmental effects on aromatic amino acid metabolism that, as discussed below, occur in four ways: (i) by redirecting flux toward other aromatic amino acids, Trp and Tyr, which share common biosynthetic precursors in plastids; (ii) by decreasing production of Phe biosynthetic precursors (e.g. shikimate) in plastids; (iii) by sequestering Phe into a metabolically inactive pool in vacuole; and (iv) by converting Phe to unknown Phe-derived compounds.

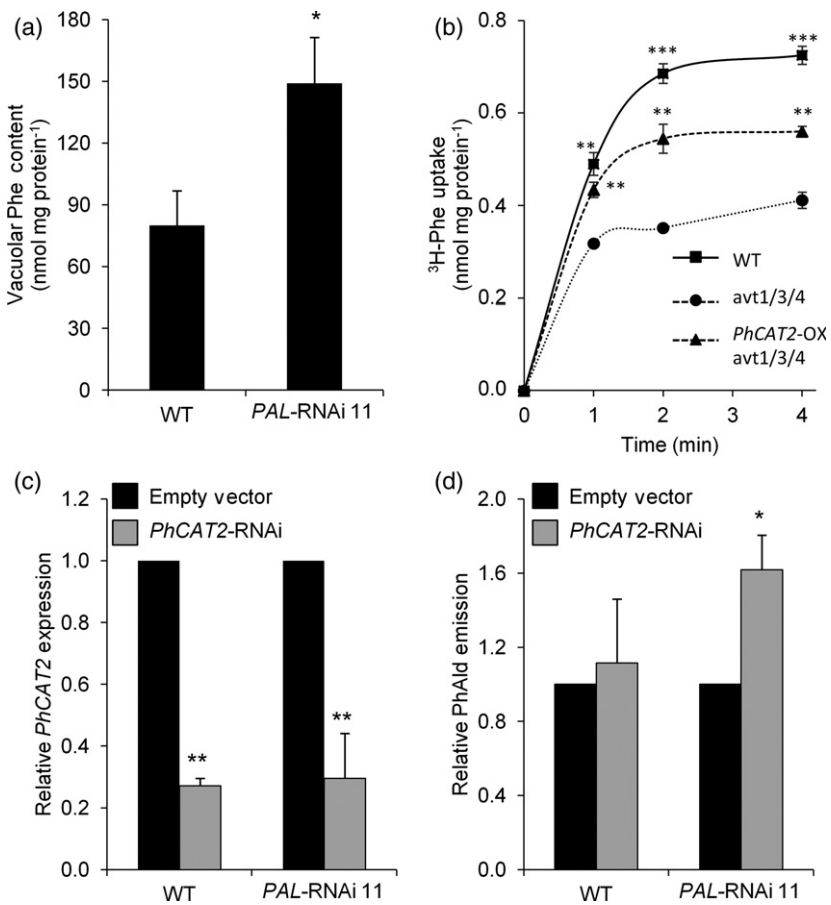

Figure 5. Effect of downregulation of vacuolar Phe transporter *PhCAT2* on phenylacetaldehyde emission in petunia flowers.
(a) Phe content of vacuoles purified from protoplasts that were isolated from wild-type and *PAL*-RNAi line 11 flower petals on 1-day post-anthesis.
(b) Phe transport assays in vacuole microsomes from wild-type BY4741 yeast (squares), the corresponding avt1/3/4 triple mutant containing the empty vector (circles) and the avt1/3/4 mutant expressing PhCAT2 (triangles), in the presence of ATP. Significance indicated relative to the avy1/3/4 triple mutant.
(c) *PhCAT2* expression in wild-type and *PAL*-RNAi line 11 flowers infiltrated with the empty vector (black bars) and the *PhCAT2* RNAi construct (gray bars).
(d) Phenylacetaldehyde emission from flowers shown in (c) over the period from 16:00 to 20:00 h. The absolute value of empty vector control emission is 2.9 and 3.2 nmol h^{-1} gFW^{-1} for wild-type and *PAL*-RNAi line 11, respectively. For all panels, data are means ± SE ($n \geq 3$ biological replicates). $^{*}P < 0.05$, $^{**}P < 0.011$, $^{***}P < 0.001$ as determined by unpaired two-tailed Student's *t*-tests.

Accumulation of Phe leads to decreased shikimate pathway flux and an increase in Tyr and Trp levels

The redirection of carbon flux towards Tyr and Trp as a result of feedback inhibition by Phe of branch-point enzymes (i.e. chorismate mutase and arogenate dehydratase) within the plastidic aromatic amino acid network has been well documented (Goers and Jensen, 1984; Eberhard *et al.*, 1996; Maeda and Dudareva, 2012; Widhalm *et al.*, 2015). Therefore, it is likely that the redirection observed in the petunia *PAL*-RNAi plants is due to expansion of the plastidial Phe pool, suggesting that Phe accumulation in the cytosol led to a decrease in its export from plastids via the PhpCAT transporter. The observed lower shikimate levels in *PAL*-RNAi plants relative to controls (Figure 1) occurred without changes in transcript abundances of shikimate pathway biosynthetic genes (Figure S5), suggesting that post-transcriptional mechanisms regulate flux through the shikimate pathway. However, to date, little is known about how the carbon flow into the shikimate pathway is regulated in plants. While in microbes DAHP synthase, which catalyzes the entry step in the shikimate pathway, is subject to feedback regulation by aromatic amino acids, such a scenario has not yet been described in plants. Given that plant DAHP synthases belong to the type II class and contain aromatic amino acid-binding elements (Webby *et al.*, 2010), it is possible that the correct conditions and/or combinations of aromatic amino acids under which plant DAHP synthase activity is affected have not yet been found. On the other hand, it is known that protein turnover of plant DAHP synthase and chorismate synthase can be regulated by the Clp protease system (Nishimura *et al.*, 2013; Nishimura and van Wijk, 2015). Recently a similar mechanism was shown to be involved in controlling accumulation of phenylpropanoids (Zhang *et al.*, 2015) and flavonoids (Feder *et al.*, 2015) via Kelch domain-containing F-box proteins. Thus, the precise mechanism(s) responsible for this observed decrease in flux through the shikimate pathway when PAL activity is decreased remain to be determined. It should be noted that for nearly two decades it has been proposed that plants synthesize salicylic acid via two parallel pathways: Phe-dependent (via benzoate) and Phe-independent (via isochorismate) pathways (Huang *et al.*, 2010). A *PAL* mutant approach was used to distinguish the contribution of these two pathways to salicylic acid biosynthesis. However, our results show that such an approach may lead

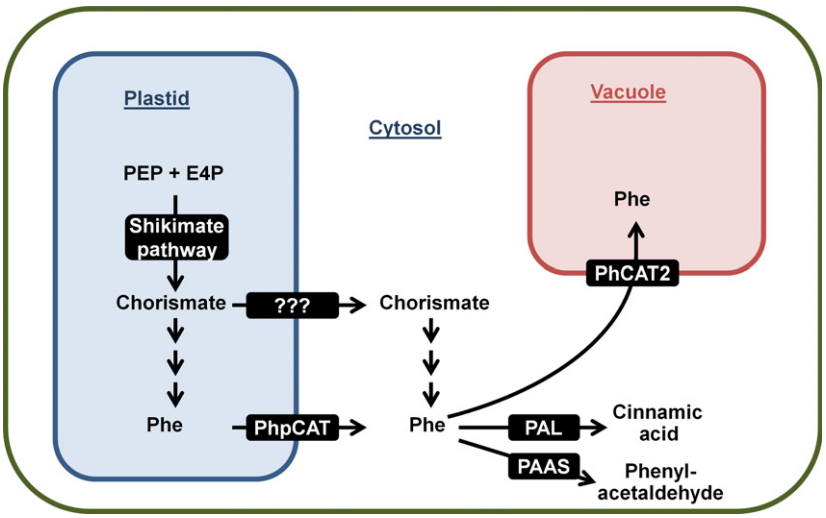

Figure 6. Proposed model of subcellular inter compartmental Phe fluxes in petunia flowers.

to misleading conclusions, as in *PAL* mutants not only the flux through the Phe-dependent pathway is reduced, but also via the Phe-independent isochorismate pathway, for which shikimate is an immediate precursor.

Some accumulated Phe is sequestered in the vacuole

Reduction of PAL activity in the plant cell is similar to PKU in mammals caused by a loss of Phe hydroxylase activity and the resulting inability to convert Phe to Tyr (Williams *et al.*, 2008). In both cases the loss of a dominant pathway for Phe consumption leads to its hyperaccumulation. Animals eliminate excess of Phe by converting it predominantly to phenylpyruvate, followed by its excretion in the urine. In contrast, plants lack the secretory system, although they contain phenylpyruvate aminotransferase, PhPPY-AT, which catalyzes the reversible conversion of phenylpyruvate to Phe (Yoo *et al.*, 2013). Phenylpyruvate levels in *PAL*-RNAi plants were unchanged relative to wild-type (Figure 1), indicating that accumulated Phe is likely unavailable for PPY-AT. Similarly, no significant differences were observed in the amount of Phe-derived metabolites, phenylacetadehyde and phenylethanol, emitted from the wild-type and *PAL*-RNAi transgenic lines ($P > 0.05$), despite the pronounced effect on cinnamic acid-derived compounds. Significantly, phenylacetaldehyde was labeled to a higher degree than its immediate substrate, Phe, after feeding with ^{13}C-glucose (Figure 4a), further suggesting the presence of a metabolically inactive Phe pool. Pulse chase experiments with $^{13}C_6$-Phe indicated a low turnover of this pool (Figure 4b), which is likely located in the vacuole (Figure 6). The presence of a small but measurable Phe pool in the vacuole was previously shown in wild-type Arabidopsis plants by non-aqueous fractionation (Krueger *et al.*, 2011) and in barley by metabolomic analysis of isolated vacuoles (Tohge *et al.*, 2011), and confirmed in petunia here (Figure 5a). Furthermore, we show that the vacuolar cationic amino acid transporter *PhCAT2* is capable of transporting Phe, and that decreasing *PhCAT2* expression in *PAL*-RNAi petunia flowers, achieved via RNAi strategy, led to an increase in the levels of the cytosolic Phe pool and subsequently in phenylacetaldehyde production (Figure 5c and d). Overall, the demonstration of this metabolically inactive pool of Phe in the vacuole provides insight into the fate of excess Phe under conditions in which its accumulation is stimulated. It also suggests a potential source of Phe for metabolic engineering strategies.

Some accumulated Phe is converted to unknown metabolites

We also noted the accumulation in petunia *PAL-RNAi* lines of three unknown compounds whose mass spectra and isotopic labeling indicate that they were derived from Phe. These compounds were present in wild-type petunia flowers at very low levels. It is not yet clear whether their accumulation is due to activation of a physiologically relevant Phe catabolic route, or merely induction of 'silent metabolism' (Lewinsohn and Gijzen, 2009) by the high Phe levels. However, both possibilities must be considered in future metabolic engineering strategies that seek to increase production of Phe and valuable downstream metabolites.

EXPERIMENTAL PROCEDURES

Vector construction

RNAi-mediated knockdown of all three PAL genes was achieved by targeting coding regions specific to PAL1 (nucleotides 923–1453, including an intron), PAL2 (nucleotides 81–440) and PAL3 (nucleotides 498–829) with a synthetic cDNA hairpin construct, generated as follows. The 1223-bp synthetic cDNA containing PAL isoforms specific regions described above was introduced into a modified pUC57 vector (pUC57-simple; Genscript, NJ, USA) to create pUC57ConA. Using pUC57ConA as a template, a shorter

fragment corresponding to nucleotides 1–1019 without intron was generated by PCR with primers RN1 and RN2 (Table S1). The amplicon was cloned between the AscI and BamHI sites of pUC57-ConA in an antisense orientation, thus completing the hairpin construct targeting all three PAL genes. The resulting hairpin fragment was released from pUC57ConA by XhoI/BamHI digestion and ligated into the corresponding sites of the modified pRNA69 vector (Orlova *et al.*, 2006) between the *Clarkia breweri* linalool synthase (LIS) petal-specific promoter and ocs terminator. The entire cassette was released by SacI/NotI digestion and ligated into the corresponding sites of the binary vector pART27.

For the *PhCAT2*-RNAi construct, DNA containing two spliced PhCAT2 cDNA fragments of the coding region corresponding to nucleotides 42–590 and 42–381, the latter in antisense orientation to create a hairpin structure, was synthesized (Genscript, NJ, USA). 5′-EcoRI and 3′-BamHI sites were added for directional subcloning into pRNA69 containing LIS promoter. The resulting cassette containing the LIS promoter and the synthetic PhCAT2 hairpin fragment was released by SacI/SpeI digestion and subcloned into the corresponding sites of the binary vector pART27.

Plant material and transformation

Petunia (*P. hybrida* cv. Mitchell, Ball Seed, http://www.ball-seed.com/) was used for the generation of transgenic plants. Plants were grown under a 16-h photoperiod in standard greenhouse conditions (Koeduka *et al.*, 2008; Maeda *et al.*, 2010). Transgenic plants were obtained via *Agrobacterium tumefaciens* (strain EHA 105 carrying plasmid pART27-ConA) leaf disk transformation (Horsch *et al.*, 1985). Plants, rooted on kanamycin selection, were screened by NPTII ELISA (Agdia, Elkhart, IN, USA, http://www.agdia.com) for neomycin phosphotransferase II, and by PCR for the presence of the LIS promoter with the specific forward and reverse primers, LIS-F and LIS-R (Table S1). T0 and T1 transformants were self-pollinated and analyzed for segregation by germinating seeds on half-strength Murashige and Skoog (MS) medium supplemented with kanamycin (200 mg L^{-1}). Untransformed petunia plants and petunia plants transformed with empty vector were used as a control in experiments, as described in results. Transient transformation was carried out by floral infiltration as described previously (Yoo *et al.*, 2013).

Arabidopsis were grown in growth chambers at 22°C and 120 μE m^{-2} s^{-1} light under a 12-h light photoperiod. Arabidopsis PAL mutants were generated previously (Huang *et al.*, 2010), and were kindly provided to us by Dr Z. Chen (Purdue University). Homozygous PAL quadruple mutants were identified by PCR using PAL2-specific primers, pal 2-2-RP and pal 2-3-RP, and T-DNA-specific primers, pal 2-2-LB and pal 2-3-LB (Table S1).

RNA extraction, cDNA synthesis and qRT-PCR

Total RNA was isolated from petal tissue using RNeasy Plant Mini Kit (Qiagene, Hilden, Germany). Each biological replicate contained a minimum of 10 2-day-old corollas harvested at 20:00 h and immediately frozen in liquid nitrogen. Total RNA was treated with DNase I using TURBO DNA-free kit (Ambion, MA, USA), and 1 μg of DNA-free RNA was reverse transcribed using the High Capacity cDNA transcription kit (Applied Biosystems, CA, USA). Gene-specific primers for each PAL gene (Table S1) were designed using PrimerExpress (Applied Biosystems, CA, USA), and showed 90–100% efficiency at a final concentration of 300 nM. qRT-PCR was performed as described previously (Maeda *et al.*, 2010). For relative quantification of *PAL1*, *PAL2* and *PAL3* transcript levels, UBQ10 was used as a reference gene (Maeda *et al.*, 2010). Each data point represents an average of three independent biological samples.

Enzyme assays

Phe ammonia lyase, PAAS and ADT activities were measured in crude protein extracts prepared from petunia petals of control and transgenic plants harvested at 20:00 h, day 2 post-anthesis as described previously (Maeda *et al.*, 2010). ADT activity was analyzed in the petunia petal plastidial fraction isolated as described before (Yoo *et al.*, 2013). Plastids were suspended in 500 μl of ADT assay buffer (250 mM sodium phosphate buffer, pH 8.2, 1 mM EDTA), metabolites were removed from soluble crude protein extracts using a Sephadex G50 column equilibrated with ADT assay buffer, and resulting proteins were assayed for ADT activity as previously described (Maeda *et al.*, 2010).

Analysis of volatiles, organic acids and aromatic amino acids

Volatile compounds were collected from control and *PAL*-RNAi petunia flowers for 12 h starting at 20:00 h 2 days post-anthesis using the closed-loop stripping method (Orlova *et al.*, 2006), and analyzed by GC-MS (Agilent, CA, USA) as described previously (Maeda *et al.*, 2010). For organic and aromatic amino acid analysis, approximately 0.5 g of frozen tissue was extracted overnight at 4°C with 10 ml of 100% methanol. A100-μl aliquot of methanol extract was analyzed at the Metabolomic Center of the University of Illinois at Urbana-Champaign for aromatic amino acids, benzoic acid, phenylpyruvic acid and shikimic acid. Chromotographic separation was achieved by high-performance liquid chromatography using a Phenyl column (100 × 4.6 mm, 3 μm) with a 6-min linear gradient of 1–95% acetonitrile in 25 mM ammonium acetate at a 0.4 ml min^{-1} flow rate. Quantification was performed using calibration curves generated from individual authentic standards.

Stable isotope labeling experiments

Corollas excised from flowers 2 days post-anthesis were placed on filter paper moistened with 2 ml of the requisite labeled compound, as described in the Results. Emitted and internal pools of volatiles were collected as described above. Phe was extracted and analyzed by LC-MS as described previously (Yoo *et al.*, 2013). Glucose and shikimate were analyzed as described previously (Maeda *et al.*, 2010), except that shikimate was extracted from tissue in 70% (v/v) methanol. The fractional labeling percentage of each compound was determined by comparison of the intensity of the shifted molecular ions and corrected for the natural isotope abundance.

Isolation of petunia vacuoles

Protoplasts were isolated from corollas of petunia flowers 1 day post-anthesis as described previously (Faraco *et al.*, 2011). Protoplasts were lysed and vacuoles were purified as described previously (Robert *et al.*, 2007), except protoplast lysis buffer contained 250 mM mannitol. Western blot analysis was performed using petal crude extracts and lyophilized vacuoles resuspended in 1 × Laemmli buffer. Immunodetection was perfomed using rabbit primary polyclonal antibodies raised against organelle-specific markers (Agrisera, Sweden). Antigen bands were visualized using Immun-Blot Goat Anti-Rabbit IgG (H + L)-AP Assay Kit (Bio-Rad) according to the manufacturer's protocol.

Yeast transport assays

AVT1, *AVT3* and *AVT4* genes, shown to be involved in amino acid transport at the vacuole (Sekito *et al.*, 2008), were deleted from *S. cerevisiae* strain BY4741 (*MAT*a *his3Δ1 leu2Δ0 met15Δ0 ura3Δ0*)

by recombination with amplicons of the *loxP-KanMX-loxP* cassette (Güldener *et al.*, 1996), *lox2272-natNT2-lox2272* and *loxLE-hphNT1-loxRE* (Carter and Delneri, 2010), respectively, generated by PCR with primers in Table S1. Gene deletions were confirmed by PCR using primers in Table S1. Yeast vacuole purification and Phe transport assays were performed according to Russnak *et al.* (2001), using PhCAT2 cloned into the gateway compatible yeast expression vector pDR196 (Loqué *et al.*, 2007).

Metabolic flux modeling

Aromatic amino acid biosynthesis was simplified as three parallel macro-reactions, each of which converts the common precursor glucose into Phe, Tyr or Trp. The equations for the three reactions focused on carbon mass balance are as follows:

$$1.67\ \text{Glucose} \xrightarrow{v_1} \text{Phe} + \text{CO}_2$$

$$1.67\ \text{Glucose} \xrightarrow{v_2} \text{Tyr} + \text{CO}_2$$

$$2\ \text{Glucose} \xrightarrow{v_3} \text{Trp} + \text{CO}_2$$

Aromatic amino acids were assumed to be the major sinks for the shikimate pathway, and therefore its flux during the feeding studies was estimated from the sum of the fluxes through those three reactions. All fluxes were assumed to be constant within a 4-h period of feeding time, and metabolite concentration dynamics in the pathway can be captured by linear functions, which matched with corresponding time course measurements. An empirical function was applied to simulate glucose labeling percentage dynamics and v1 was constrained by known Phe-derived volatile emission rates. Inclusion of a metabolically inactive pool parameter for Phe improved fit with experimental observations. In total, 11 unknown parameters were estimated for each case. Detailed involvements of these parameters into the model are listed below:

$$C_{\text{Phe}_{\text{interactive},\,t}} = \theta_1 + \frac{\theta_2 - \theta_1}{4} * t$$

$$C_{\text{Tyr}_t} = \theta_3 + \frac{\theta_4 - \theta_3}{4} * t$$

$$C_{\text{Trp}_t} = \theta_5 + \frac{\theta_6 - \theta_5}{4} * t$$

$$f_{\text{Glucose}_t} = \theta_7 * (1 - e^{-\theta_8 * t})$$

$$v_1 = v_{\text{emission}} + \frac{\theta_2 - \theta_1}{4}$$

$$v_2 = \theta_9$$

$$v_3 = \theta_{10}$$

$$C_{\text{Phe}_{\text{uninteractive}}} = \theta_{11}$$

For each aromatic amino acid, labeling percentage dynamics were numerically integrated with the following balance equations (Widhalm *et al.*, 2015) by ode15 solver in Matlab R2013a (The MathWorks, Natick, MA, USA):

$$\frac{df_{\text{Phe}_{\text{interactive},\,t}}}{dt} = \frac{(f_{\text{Glucose}_t} - f_{\text{Phe}_{\text{interactive},\,t}}) * v_1}{C_{\text{Phe}_{\text{interactive},\,t}}}$$

$$\frac{df_{\text{Tyr}_t}}{dt} = \frac{(f_{\text{Glucose}_t} - f_{\text{Tyr}_t}) * v_2}{C_{\text{Tyr}_t}}$$

$$\frac{df_{\text{Trp}_t}}{dt} = \frac{(f_{\text{Glucose}_t} - f_{\text{Trp}_t}) * v_3}{C_{\text{Trp}_t}}$$

To enable direct comparison of the model's outputs with experimental measurements, the metabolically inactive Phe pool was integrated into the final outputs as follows:

$$C_{\text{Phe}_t} = C_{\text{Phe}_{\text{interactive},\,t}} + C_{\text{Phe}_{\text{uninteractive},\,t}}$$

$$f_{\text{Phe}_t} = f_{\text{Phe}_{\text{interactive},\,t}} * \frac{C_{\text{Phe}_{\text{interactive},\,t}}}{C_{\text{Phe}_t}}$$

The objective function was defined as the differences between model-predicted profiles and experimentally measured profiles, weighed by the measurement variances. Parameters were estimated by minimizing the objective function through lsqnonlin function in Matlab R2013a with multi-run approach. The mathematical representation of the optimization process is shown below:

$$\theta = arg\min_{\theta} \sum \frac{(\text{Profile}_{\text{simulated}} - \text{Profile}_{\text{measured}})^2}{s^2_{\text{Profile}_{\text{measured}}}}$$

Parameter uncertainty analysis was also performed as described in Press (2007). Briefly, 5000 synthetic datasets were generated based on average and variance for each measurement by assuming a Gaussian distribution. For each dataset, the same optimization process was performed to obtain parameter values, and parameter uncertainty as well as model-predicted profile variance was estimated based on the variance of 5000 parameter sets.

Subcellular localization of PhCAT2

The full-length coding sequence of PhCAT2 was amplified using forward and reverse primers, PhCAT2-F and PhCAT2-NSR, respectively (Table S1), both of which include primer extensions for SfiI recognition sites. The resulting fragment was subcloned into SfiI sites of pENTR223, sequence verified and transferred into pK7FWG2 via GatewayTM technology, resulting in an in-frame fusion with the N-terminal end of GFP. The *PhCAT2*-GFP construct was stably transformed via Agrobacterium-mediated floral dip into *A. thaliana* expressing the tonoplast marker VAMP711-mCHERRY (Geldner *et al.*, 2009). T1 plants surviving kanamycin selection were imaged. Images were acquired using a Zeiss LSM710 laser spectral scanning confocal microscope with a C-Apochromat 40× /1.20 W objective (Zeiss, NY, USA). GFP was excited with an argon laser at wavelength 488 nm, and emissions were collected over a 493–598 nm bandpass. mCherry was excited at wavelength 561 nm, and emissions were collected over 600–680 nm bandpass. Chlorophyll fluorescence was excited by a HeNe laser at wavelength 633 nm and emissions were collected over a 647–721 nm bandpass.

ACCESSION NUMBERS

The GenBank/EMBL accession number for the sequence mentioned in this article is as follows: KX817349.

ACKNOWLEDGEMENTS

This work was supported by a grant from the National Science Foundation MCB-1519083 to ND. The authors thank Dr Zhixiang Chen for providing seeds of Arabidopsis *pal* mutants, and Dr Francesca Quattrocchio and Shuanjiang Li for advising on the isolation of protoplasts.

CONFLICT OF INTEREST

The authors declare no conflict of interest.

SUPPORTING INFORMATION

Additional Supporting Information may be found in the online version of this article.

Figure S1. Protein sequence alignment for the three *Petunia hydrida*, cv. Mitchell PAL isoforms.

Figure S2. Generation of petunia *PAL* RNAi lines.

Figure S3. Metabolic analysis of empty vector control petunia flowers.

Figure S4. Isotopic abundances and pool sizes of shikimate in control and *PAL*-RNAi petunia flowers during feeding with [U-$^{13}C_6$]-glucose.

Figure S5. Expression levels of genes encoding enzymes involved in aromatic amino acid biosynthesis and ODO1 transcription factor in control and *PAL*-RNAi petunia flowers.

Figure S6. Model simulated and experimentally determined phenylacetaldehyde emission in transgenic *PAL*-RNAi flowers.

Figure S7. Representative Western blot analysis of purity of isolated vacuoles.

Figure S8. Subcellular localization of PhCAT2.

Figure S9. ATP dependence of Phe transport by yeast vacuolar microsomes.

Figure S10. Representative GC-MS chromatograms of trimethylsilyl (TMS)-derived extracts obtained from control and *PAL*-RNAi petunia flowers.

Table S1. Sequences of primers used for cloning, genotyping and qRT-PCR.

REFERENCES

Bentley, R. (1990) The shikimate pathway – metabolic tree with many branches. *Crit. Rev. Biochem. Mol. Biol.* **25**, 307–383.

Boatright, J., Negre, F., Chen, X., Kish, C.M., Wood, B., Peel, G., Orlova, I., Gang, D., Rhodes, D. and Dudareva, N. (2004) Understanding in vivo benzenoid metabolism in petunia petal tissue. *Plant Physiol.* **135**, 1193–2011.

Brouquisse, R., James, F., Pradet, A. and Raymond, P. (1992) Asparagine metabolism and nitrogen distribution during protein degradation in sugar-starved maize root-tip. *Planta*, **188**, 384–395.

Carter, Z. and Delneri, D. (2010) New generation of loxP-mutated deletion cassettes for the genetic manipulation of yeast natural isolates. *Yeast*, **27**, 765–775.

Cass, C.L., Antoine, P. and Dowd, P.F. (2015) Effects of phenylalanine ammonia lyase (PAL) knockdown on cell wall composition, biomass digestibility, and biotic and abiotic stress responses in Brachypodium. *J. Exp. Bot.* **66**, 4317–4335.

Colón, A.M., Sengupta, N., Rhodes, D., Dudareva, N. and Morgan, J. (2010) A kinetic model describes metabolic response to perturbations and distribution of flux control in the benzenoid network of Petunia hybrida. *Plant J.* **62**, 64–76.

Cseke, L., Dudareva, N. and Pichersky, E. (1998) Structure and evolution of linalool synthase. *Mol. Biol. Evol.* **15**, 1491–1498.

Eberhard, J., Ehrler, T.T., Epple, P., Felix, G., Raesecke, H., Amrhein, N. and Schmid, J. (1996) Cytosolic and plastidic chorismate mutase isozymes from Arabidopsis thaliana: molecular characerization and enzymatic properties. *Plant J.* **10**, 815–821.

Faraco, M., Sansebastiano, G.P.D., Spelt, K., Koes, R.E. and Quattrocchio, F.M. (2011) One protoplast is not the other!. *Plant Physiol.* **156**, 474–478.

Feder, A., Burger, J. and Gao, S. (2015) A Kelch domain-containing F-box coding gene negatively regulates flavonoid accumulation in muskmelon. *Plant Physiol.* **169**, 1714–1726.

Fuchs, G., Boll, M. and Heider, J. (2011) Microbial degradation of aromatic compounds – from one strategy to four. *Nat. Rev. Microbiol.* **9**, 803–816. Available at: https://doi.org/10.1038/nrmicro2652.

Geldner, N., Denervaud-Tendon, V., Hyman, D.L., Mayer, U., Stierhof, Y. and Chory, J. (2009) Rapid, combinatorial analysis of membrane compartments in intact plants with a multicolor marker set. *Plant J.* **59**, 169–178.

Goers, S.K. and Jensen, R.A. (1984) The differential allosteric regulation of two chorismate-mutase isoenzymes of Nicotiana silvestris. *Planta*, **162**, 117–124.

Güldener, U., Heck, S., Fiedler, T., Beinhauer, J. and Hegemann, J.H. (1996) A new efficient gene disruption cassette for repeated use in budding yeast. *Nucleic Acids Res.* **24**, 2519–2524.

Haslam, E. (1993) *Shikimic Acid: Metabolism and Metabolites*. Chichester: John Wiley.

Herrmann, K.M. and Weaver, L.M. (1999) The shikimate pathway. *Ann. Rev. Plant Physiol. Plant Mol. Biol.* **50**, 473–503.

Homeyer, U. and Schultz, G. (1988) Transport of phenylalanine into vacuoles isolated from barley mesophyll protoplasts. *Planta*, **176**, 378–382.

Horsch, R.B., Fry, J.E., Hoffmann, N.L., Eichholtz, D., Rogers, S.G. and Fraley, R.T. (1985) A simple and general method for transferring genes into plants. *Science*, **227**, 1229–1231.

Huang, J., Gu, M., Lai, Z., Fan, B., Shi, K., Zhou, Y., Yu, J. and Chen, Z. (2010) Functional analysis of the Arabidopsis PAL gene family in plant growth, development, and response to environmental stress. *Plant Physiol.* **153**, 1526–1538.

Kaminaga, Y., Schnepp, J. and Peel, G. (2006) Plant phenylacetaldehyde synthase is a bifunctional homotetrameric enzyme that catalyzes phenylalanine decarboxylation and oxidation. *J. Biol. Chem.* **281**, 23357–23366.

Kim, D.S. and Hwang, B.K. (2014) An important role of the pepper phenylalanine ammonia-lyase gene (PAL1) in salicylic acid-dependent signalling of the defence response to microbial pathogens. *J. Exp. Bot.* **65**, 2295–2306.

Kim, S.W., Koo, B.C., Kim, J. and Liu, J.R. (2007) Metabolic discrimination of sucrose starvation from Arabidopsis cell suspension by 1H NMR based metabolomics. *Biotechnol. Bioprocess Eng.* **12**, 653–661.

Koeduka, T., Louie, G.V. and Orlova, I. (2008) The multiple phenylpropene synthases in both Clarkia breweri and Petunia hybrida represent two distinct protein lineages. *Plant J.* **54**, 362–374.

Krueger, S., Giavalisco, P., Krall, L., Steinhauser, M., Bussis, D., Usadel, B., Flugge, U., Fernie, A.R., Willmitzer, L. and Steinhauser, D. (2011) A topological map of the compartmentalized Arabidopsis thaliana leaf metabolome. *PLoS One*, **6**, e17806.

Lewinsohn, E. and Gijzen, M. (2009) Phytochemical diversity: the sounds of silent metabolism. *Plant Sci.* **176**, 161–169.

Loqué, D., Lalonde, S., Looger, L.L., von Wiren, N. and Frommer, W.B. (2007) A cytosolic trans-activation domain essential for ammonium uptake. *Nature*, **446**, 195–198.

Maeda, H. and Dudareva, N. (2012) The shikimate pathway and aromatic amino acid biosynthesis in plants. *Ann. Rev. Plant Biol.* **63**, 73–105.

Maeda, H., Shasany, A.K., Schnepp, J., Orlova, I., Taguchi, G., Cooper, B.R., Rhodes, D., Pichersky, E. and Dudareva, N. (2010) RNAi suppression of arogenate dehydratase1 reveals that phenylalanine is synthesized predominantly via the arogenate pathway in petunia petals. *Plant Cell*, **22**, 832–849.

Nishimura, K. and van Wijk, K.J. (2015) Organization, function and substrates of the essential Clp protease system in plastids. *Biochim. Biophys. Acta*, **1847**, 915–930 Available at: https://doi.org/10.1016/j.bbabio.2014.11.012.

Nishimura, K., Asakura, Y., Friso, G., Kim, J., Oh, S., Rutschow, H., Ponnala, L. and van Wijk, K.J. (2013) ClpS1 is a conserved substrate selector for the chloroplast Clp protease system in Arabidopsis. *Plant Cell*, **25**, 2276–2301. Available at: http://www.ncbi.nlm.nih.gov/pubmed/23898032.

Orlova, I., Marshall-Colon, A. and Schnepp, J. (2006) Reduction of benzenoid synthesis in petunia flowers reveals multiple pathways to benzoic acid and enhancement in auxin transport. *Plant Cell*, **18**, 3458–3475.

Press, W.H. (2007) *Numerical Recipes: The Art of Scientific Computing*, 3rd edn. New York: Cambridge University Press.

Raes, J., Rohde, A., Christensen, J.H., Van de Peer, Y. and Boerjan, W. (2003) Genome-wide characterization of the lignification toolbox in Arabidopsis. *Plant Physiol.* **133**, 1051–1071. Available at: http://www.scopus.com/inward/record.url?eid=2-s2.0-0142035247&partnerID=40&md5=e4e081e08156acbc208e15a29bc16846%5Cnhttp://www.plantphysiology.org/content/133/3/1051.full%5Cnhttp://www.plantphysiology.org/content/133/3/1051.short.

Razal, R.A., Ellis, S., Singh, S., Lewis, N.G. and Towers, G.H.N. (1996) Nitrogen recycling in phenylpropanoid metabolism. *Phytochemistry*, **41**, 31–35.

Reichert, A.I., He, X. and Dixon, R.A. (2009) Phenylalanine ammonia-lyase (PAL) from tobacco (Nicotiana tabacum): characterization of the four tobacco PAL genes and active heterotetrameric enzymes. *Biochem. J.* **242**, 233–242.

Robert, S., Zouhar, J., Carter, C. and Raikhel, N. (2007) Isolation of intact vacuoles from Arabidopsis rosette leaf-derived protoplasts. *Nat. Prot.* **2**, 259–262.

Rohde, A., Morreel, K., Ralph, J. and Goeminne, G. (2004) Molecular phenotyping of the pal1 and pal2 mutants of Arabidopsis thaliana reveals far-reaching consequences on phenylpropanoid, amino acid, and carbohydrate metabolism. *Plant Cell*, **16**, 2749–2771.

Russnak, R., Konczal, D. and McIntire, S.L. (2001) A family of yeast proteins mediating bidirectional vacuolar amino acid transport. *J. Biol. Chem.* **276**, 23849–23857.

Saeedipour, S. and Moradi, F. (2012) Stress-induced changes in the free amino acid composition of two wheat cultivars with difference in drought resistance. *Afr. J. Biotechnol.* **11**, 9559–9565.

Sekito, T., Fujiki, Y., Ohsumi, Y. and Kakinuma, Y. (2008) Novel families of vacuolar amino acid transporters. *IUBMB Life*, **60**, 519–525.

Shi, R., Yank, C., Lu, S., Sederoff, R. and Chiang, V.L. (2010) Specific down-regulation of PAL genes by artificial microRNAs in populus trichocarpa. *Planta*, **232**, 1281–1288.

Song, J. and Wang, Z. (2011) RNAi-mediated suppression of the phenylalanine ammonia-lyase gene in Salvia miltiorrhiza causes abnormal phenotypes and a reduction in rosmarinic acid biosynthesis. *J. Plant. Res.* **124**, 183–192.

Su, Y., Frommer, W.B. and Ludewig, U. (2004) Molecular and functional characterization of a family of amino acid transporters from Arabidopsis. *Plant Physiol.* **136**, 3104–3113.

Tohge, T., Ramos, M.S. and Nunes-Nesi, A. (2011) Toward the storage metabolome: profiling the barley vacuole. *Plant Physiol.* **157**, 1469–1482.

Verdonk, J.C., de Vos, C.H.R., Verhoeven, H.A., Haring, M.A., van Tunen, A.J. and Schuurink, R.C. (2003) Regulation of floral scent production in petunia revealed by targeted metabolomics. *Phytochemistry*, **62**, 997–1008.

Verdonk, J.C., Haring, M.A., van Tunen, A.J. and Schuurink, R.C. (2005) ODORANT1 regulates fragrance biosynthesis in petunia flowers. *Plant Cell*, **17**, 1612–1624.

Webby, C.J., Jiao, W., Hutton, R.D., Blackmore, N.J., Baker, H.M., Baker, E.N., Jameson, G.B. and Parker, E.J. (2010) Synergistic allostery, a sophisticated regulatory network for the control of aromatic amino acid biosynthesis in Mycobacterium tuberculosis. *J. Biol. Chem.* **285**, 30567–30576.

Widhalm, J.R., Gutensohn, M. and Yoo, H. (2015) Identification of a plastidial phenylalanine exporter that influences flux distribution through the phenylalanine biosynthetic network for bioenergy. *Nat. Commun.* **6**, 8142.

Williams, R.A., Mamotte, C.D.S. and Burnett, J.R. (2008) Phenylketonuria: an inborn error of phenylalanine metabolism. *Clin. Biochem.* **29**, 31–41.

Yang, H., Krebs, M., Stierhof, Y. and Ludewig, U. (2014) Characterization of the putative amino acid transporter genes AtCAT2, 3 & 4: the tonoplast localized AtCAT2 regulates soluble leaf amino acids. *J. Plant Physiol.* **171**, 594–601. Available at: https://doi.org/10.1016/j.jplph.2013.11.012.

Yoo, H., Widhalm, J.R., Qian, Y., Maeda, H., Cooper, B.R., Jannasch, A.S., Gonda, I, Lewinsohn, E., Rhodes, D. and Dudareva, N. (2013) An alternative pathway contributes to phenylalanine biosynthesis in plants via a cytosolic tyrosine: phenylpyruvate aminotransferase. *Nat. Commun.* **4**, 2833. Available at: https://doi.org/10.1038/ncomms3833.

Zhang, X. and Liu, C. (2015) Multifaceted regulations of gateway enzyme phenylalanine ammonia-lyase in the biosynthesis of phenylpropanoids. *Mol. Plant*, **8**, 17–27. Available at: https://doi.org/10.1016/j.molp.2014.11.001.

Zhang, X., Gou, M., Guo, C., Yank, H. and Liu, C. (2015) Down-regulation of Kelch domain-containing F-box protein in Arabidopsis enhances the production of (poly)phenols and tolerance to ultraviolet radiation. *Plant Physiol.* **167**, 337–350.